Wind-Generated Power Input to the Deep Ocean: An Estimate Using a 1/10° General Circulation Model

JIN-SONG VON STORCH

Max Planck Institute for Meteorology, Hamburg, Germany

HIDEHARU SASAKI

Earth Simulator Center, Yokohama, Japan

JOCHEM MAROTZKE

Max Planck Institute for Meteorology, Hamburg, Germany

(Manuscript received 14 October 2005, in final form 20 June 2006)

ABSTRACT

Recent studies on the wind-generated power input to the geostrophic and nongeostrophic ocean circulation components have used expressions derived from Ekman dynamics. The present work extends and unifies previous studies by deriving an expression from the kinetic energy budget of the upper layer based on the primitive equations. Using this expression, the wind-generated power available to the deep ocean is estimated from an integration with the 1/10° ocean general circulation model of the Earth Simulator Center. The result shows that the total power generated by the wind at the sea surface is about 3.8 TW. About 30% of this power (1.1 TW) is passed through a surface layer of about 110-m thickness to the ocean beneath. Approximating the wind-generated power to the deep ocean using Ekman dynamics produces two large errors of opposite signs, which cancel each other to a large extent.

1. Introduction

The oceanic meridional overturning circulation (MOC) is thought to result from downwelling into the deep ocean in localized regions and upwelling throughout the rest of the deep ocean. The MOC requires on the order of 2 TW (10^{12} W) of power to turbulently warm the abyssal waters so that they can upwell (Munk and Wunsch 1998). This energy input is thought to be supplied by the wind and the tides.

Recently, several studies have been carried out to assess the source of mechanical energy provided by the wind. These studies can be divided into two types. The first one equates the wind-generated power to the scalar product of the wind stress with the surface *geostrophic* flow (Wunsch 1998). Integrated over a constant level surface beneath the Ekman layer, this power can be interpreted as the rate of energy transferred downward beneath the Ekman layer by the pressure via the Ekman pumping velocity (Stern 1975). Using the wind stress from the National Centers for Environmental Prediction (NCEP) and the surface geostrophic flow estimated from the satellite altimeter data, Wunsch estimated the amount of this power as 1.3 TW.

The second type of consideration equates the wind power to the scalar product of the wind stress with the surface *nongeostrophic* flow. For instance, Wang and Huang (2004) estimated the power input by the wind to the surface ageostrophic currents by calculating the product between the wind stress and the ageostrophic surface velocity using an empirical formula based on the classical Ekman spiral solution (Wang and Huang 2004). They obtained values around 2.3 TW. Also belonging to the second type of consideration is the consideration of the power input to the near-inertial motions by Alford (2001) and Watanabe and Hibiya (2002). These authors calculated the power from the product of the wind stress with the velocity of the near-inertial motions obtained from slab models. In contrast

Corresponding author address: Jin-Song von Storch, Max Planck Institute for Meteorology, Bundesstrasse 53, D-20146 Hamburg, Germany.
E-mail: jin-song.von.storch@zmaw.de

DOI: 10.1175/JPO3001.1

to the first type, the power estimated by the second type "is likely to be spent on supporting turbulence and mixing in the Ekman layer and thus maintains the velocity and stratification field in the upper ocean" (Wang and Huang 2004). Even though the second type of consideration can, in conjunction with the first type, provide information about the total amount of the power generated by the wind, it does not identify the fraction of the total power that is available to the deep ocean.

Given that the power generated by the wind represents a major source of the mechanical energy required to maintain the MOC, a more complete consideration that extends and unifies the previous studies is desirable. Such a contribution is presented here. It utilizes a more comprehensive definition of the wind-generated power available to the deep ocean. The definition is derived from the kinetic energy budget of an upper layer of the ocean. Different from the previous studies, the present paper explicitly differentiates between the total power generated by the wind and the portion of the total power that is passed to the deeper ocean below a surface layer. The consideration is more complete in the sense that it is based on the primitive equations.

Evaluating the wind-generated power input using the more comprehensive definition requires three-dimensional fields of velocity and density. Because these fields are not directly available from observations, this paper makes use of a recently completed integration performed with a global ocean general circulation model with $\frac{1}{10}^\circ$ horizontal resolution. A model at such a resolution is believed to provide a more complete representation of the range of motion described by the primitive equations. Thus, the use of the $\frac{1}{10}^\circ$ model can better serve the purpose of identifying the differences between the consideration based on the primitive equations and those based on the simpler Ekman dynamics.

Section 2 describes the model data used. A more comprehensive definition of the power available to the deep ocean is derived from the time-averaged kinetic energy budget of an upper layer of the ocean in section 3. After a short discussion on the ability of the model to reproduce observations in section 4a, the power that is passed through a surface layer is analyzed in sections 4b and 4c. Errors related to the consideration by Wunsch are discussed in section 4d. Conclusions are given in section 5.

2. Model data used

The ocean model used is the OGCM for the earth simulator (OFES). It is based on the Modular Ocean Model (MOM) 3 on a Mercator grid (Pacanowski and Griffies 2000) with significant modifications on the parallelization procedures. The model covers a near-global region extending from 75°S to 75°N with 54 vertical levels and a horizontal grid spacing of 0.1°. The model has a free surface. After a spin-up run of 50 yr (Masumoto et al. 2004), an integration is performed using the daily surface fluxes derived from the NCEP reanalysis for the period from 1950 to 2003. The sensible and latent heat fluxes are diagnosed from air temperature, relative humidity, total cloud cover, surface wind speed, and model SST using a bulk formula (Rosati and Miyakoda 1988). The longwave heat flux is parameterized following Budyko (1974). The shortwave heat flux is taken from NCEP daily mean values. The surface freshwater flux is obtained from the NCEP daily mean precipitation and the evaporation estimated from the latent heat flux, plus a restoring term with a restoring time scale of 6 days for the first model layer of 5-m thickness. There is no temperature restoration. The wind stress is taken from the NCEP daily mean values.

The restoring in the surface freshwater flux may affect the budgets of the internal and gravitational potential energy. However, because the present consideration concentrates on the budget of kinetic energy, the effect resulting from restoring in the freshwater flux is believed to be secondary.

The OFES output is stored as snapshots on every third day. Because the present study focuses on the power generated by the wind that penetrates through the upper layer, the first 14 levels from 5 m down to 114 m are considered. Because of difficulties in transferring the huge amount of data, only the last 5 yr of the OFES integration are analyzed. When interpreting the result, one should keep in mind that these data are unable to capture contributions from variations on time scales longer than 5 yr.

It is well known that the spectra of sampled processes, such as the 3-day snapshots of the OFES output, are contaminated by aliasing errors (Priestley 1981). The appendix shows that even though the spectra of (cross-spectra between) the sampled processes are contaminated by aliasing errors, the contamination is under most circumstances such that the total variances (covariances) of the sampled processes are identical to the total variances (covariances) of the original unsampled processes. Because the present paper concentrates on the total mean kinetic energy, which represents the total variance of velocity, rather than the frequency decomposition of the kinetic energy, the use of the snapshots should not be a problem.

3. Budget of the kinetic energy of a surface layer

The budget of the kinetic energy per unit volume, as derived from the primitive equations with the Boussinesq approximation, reads

$$\frac{\partial e}{\partial t} = -\nabla_3 \cdot (e\mathbf{u}_3) - \nabla_3 \cdot (p\mathbf{u}_3) + \frac{\partial}{\partial z}(\mathbf{u} \cdot \tau) - gw\rho + \nabla \cdot (\mu \nabla e) - \epsilon, \quad (1)$$

where ∇_3 (∇) is the three-dimensional (two-dimensional) gradient operator, $\mathbf{u}_3$ is the three-dimensional velocity vector with components (u, v, w), and $\mathbf{u}$ is the horizontal velocity with component (u, v); e is equal to $(\frac{1}{2})\rho_0 \mathbf{u} \cdot \mathbf{u}$, and p is pressure, ρ is the density, g is the gravity, $\tau = (\tau_x, \tau_y)$ is the horizontal stress, μ is the horizontal viscosity coefficient, and ϵ is the viscous dissipation, which is always positive.

Generally, e represents kinetic energy resulting from a broad range of variations and Eq. (1) does not necessarily have a steady solution. Consequently, one should consider the time-averaged budget, rather than the steady solution of Eq. (1). In the following, Eq. (1) is averaged over time. The time averages are denoted by an overbar. Integrating Eq. (1) over the volume of a surface layer extending from the sea surface to depth d and averaging the result over time yields

$$0 = \frac{\partial \mathcal{E}}{\partial t} = \mathcal{J}_d + \mathcal{P}_d + \mathcal{F} + \mathcal{C} - \mathcal{D}. \quad (2)$$

Here $\mathcal{E}$ is the volume integral of $\bar{e}$, representing the time mean kinetic energy in the layer. Denoting variables at the sea surface and at the depth d by the subscripts s and d, respectively, the time rate of change of $\mathcal{E}$ is determined by the sum of the following five terms: $\mathcal{J}_d$, $\mathcal{P}_d$, $\mathcal{F}$, $\mathcal{C}$, and $\mathcal{D}$. The volume integral of the last term in Eq. (1) is $\mathcal{D}$. The volume integral of the second-to-last term in Eq. (1) vanishes. The volume integral of the first three terms on the right-hand side of Eq. (1) results in $\mathcal{J}_d$, $\mathcal{P}_d$, and $\mathcal{F}$, respectively, which are further described below.

Denote the vertical integral from d to the sea surface η by $\int_d^\eta dz$ and the area integral by $\int_A dA$. The volume integral of the divergence of $e\mathbf{u}_3$, the first term on the right-hand side of Eq. (1), gives

$$\mathcal{J}_d = \int_A \overline{e_d w_d}\, dA. \quad (3)$$

Here $e\mathbf{u}_3$ is the three-dimensional flux of kinetic energy. Assuming that this flux vanishes at the sea surface and the coastal boundaries, meaning that the currents do not transport kinetic energy out of the ocean, the volume integral reduces to the area integral of the vertical energy flux ew across the level surface at d.

The volume integral of the divergence of $p\mathbf{u}_3$, the second term on the right-hand side of Eq. (1), gives the power generated by the pressure

$$\mathcal{P}_d = \int_A \overline{p_d w_d}\, dA. \quad (4)$$

Equation (4) is obtained by assuming that p is zero at the sea surface and the horizontal velocity vanishes at the coastal boundary. The volume integral of $\nabla \cdot p\mathbf{u}_3$ reduces then to the area integral of the power generated by the pressure via the vertical velocity at level d. The expression of $\mathcal{P}_d$ can be reformulated using

$$w_d = w_s + \int_d^\eta \nabla \cdot \mathbf{u}\, dz = w_s + \nabla \cdot \mathbf{U} - \mathbf{u}_s \cdot \nabla \eta, \quad (5)$$

where $\mathbf{U} = \int_d^\eta \mathbf{u}\, dz$ is the vertically integrated horizontal velocity, also referred to as the near-surface transport. Equation (5) results from vertically integrating the condition of $\nabla_3 \cdot \mathbf{u}_3$. The last term in Eq. (5) results from exchanging operators $\int dz$ and ∇ according to Leibnitz's rule. Using the surface kinematic boundary condition, one has

$$w_s = \frac{\partial \eta}{\partial t} + \mathbf{u}_s \cdot \nabla \eta. \quad (6)$$

Substituting Eq. (5) with Eq. (6) into Eq. (4) yields

$$\mathcal{P}_d = \mathcal{P}_{d,1} + \mathcal{P}_{d,2}, \quad (7)$$

where

$$\mathcal{P}_{d,1} = \int_A \overline{p_d \frac{\partial \eta}{\partial t}}\, dA \quad (8)$$

is the contribution from $(\partial \eta / \partial t)$ and

$$\mathcal{P}_{d,2} = \int_A p_d \nabla \cdot \mathbf{U}\, dA = -\int_A \overline{\mathbf{U} \cdot \nabla p_d}\, dA \quad (9)$$

is the contribution from the divergence of the near-surface transport. In the derivation of Eq. (9), an integration by parts is used under the assumption of vanishing $\mathbf{U}$ at the lateral boundaries.

The volume integral of the third term on the right-hand side of Eq. (1) results in

$$\mathcal{F} = \mathcal{F}_s - \mathcal{F}_d = \int_A \overline{\mathbf{u}_s \cdot \tau_s}\, dA - \int_A \overline{\mathbf{u}_d \cdot \tau_d}\, dA, \quad (10)$$

where $\mathcal{F}_s$ represents the power generated by the surface wind stress τ_s and $\mathcal{F}_d$ is the power generated by the stress τ_d at d with

$$\tau_d = -\rho_o K_m \frac{\partial \mathbf{u}}{\partial z}. \quad (11)$$

In the OFES model, the vertical viscous diffusivity K_m is produced by the nonlocal K profile parameterization

TABLE 1. Terms that give the wind-generated power at the sea surface $\mathcal{F}_s$ and the wind-generated power exported from the surface layer of thickness d to the ocean beneath $\mathcal{W} = \mathcal{J}_d + \mathcal{P}_{d,1} + \mathcal{P}_{d,2} - \mathcal{F}_d$; $\mathcal{P}_{\text{wunsch}}$ is an approximation of $\mathcal{W}$ used by Wunsch (1998).

Symbol	Definition	Meaning
$\mathcal{J}_d$	$\int_A \overline{e_d w_d}\, dA$	Vertical kinetic energy flux across d; $e_d = (\frac{1}{2})\rho_0 \mathbf{u}_d \cdot \mathbf{u}_d$ is the kinetic energy per unit volume and w_d is the vertical velocity at d
$\mathcal{F}$	$\mathcal{F}_s - \mathcal{F}_d$	Difference between the power generated by stress at the surface and that at the bottom of the layer
$\mathcal{F}_s$	$\int_A \overline{\mathbf{u}_s \cdot \tau_s}\, dA$	Power generated by wind stress τ_s at the sea surface; $\mathbf{u}_s$ is the horizontal velocity at the sea surface
$\mathcal{F}_d$	$\int_A \overline{\mathbf{u}_d \cdot \tau_d}\, dA$	Power generated by shear-induced stress τ_d at d; $\mathbf{u}_d$ is the horizontal velocity at depth d
$\mathcal{P}_d$	$\int_A \overline{p_d w_d}\, dA$	Power generated by the product of pressure p_d and the vertical velocity w_d
$\mathcal{P}_{d,1}$	$\int_A \overline{p_d(\partial\eta/\partial t)}\, dA$	Power generated by the product of pressure p_d and the part of w_d originating from variations of SSH η
$\mathcal{P}_{d,2}$	$-\int_A \overline{\mathbf{U} \cdot \nabla p_d}\, dA$	Power generated by the product of pressure p_d and the part of w_d originating from the (divergence of) vertically integrated horizontal velocity $\mathbf{U}$
$\mathcal{W}$	$\mathcal{J}_d + \mathcal{P}_{d,1} + \mathcal{P}_{d,2} - \mathcal{F}_d$	Power exported from the surface layer to the ocean beneath d
$\mathcal{P}_{\text{wunsch}}$	$-\int_A (\overline{\tau_{s,x} u_{g,\eta}} + \overline{\tau_{s,y} v_{g,\eta}})\, dA$	Approximation of $\mathcal{W}$ used by Wunsch; $(\tau_{s,x}, \tau_{s,y})$ represents wind stress τ_s, $(u_{g,\eta}, v_{g,\eta})$ the geostrophic velocity derived from η

(KPP) (Large et al. 1994) and varies both horizontally and vertically.

Last, volume integrating the forth term on the right-hand side of Eq. (1) leads to the conversion between potential and kinetic energy in the layer

$$C = -\int_d^\eta \int_A g\, \overline{\rho w}\, dA\, dz. \tag{12}$$

The kinetic energy budget of the surface layer of depth d suggests that $\mathcal{F}_s$ is the power provided by the wind at the top of the layer, C is the power dissipated and $\mathcal{D}$ is the power converted to potential energy within the layer, and

$$\mathcal{W} \equiv \mathcal{J}_d + \mathcal{P}_d - \mathcal{F}_d = \mathcal{J}_d + \mathcal{P}_{d,1} + \mathcal{P}_{d,2} - \mathcal{F}_d \tag{13}$$

is the power that passes through the surface layer and becomes available to the deep ocean. Terms in Eq. (13), and an approximation of $\mathcal{W}$ to be discussed below, will be estimated using the OFES data. For the sake of clarity, they are summarized in Table 1.

The classification of the power put into, and that which remained in and passed to the ocean beneath the surface layer, is based on the following consideration. When dividing the ocean into two layers with an interface at d and formulating the kinetic energy budgets for each layer, it can be shown that $\mathcal{W}$ appears with a minus sign in the budget of the lower layer, whereas $\mathcal{D}$ and C calculated from the variables in the upper layer do not appear in the budget of the lower layer. In this sense, $\mathcal{D}$ and C give the amount of power that remains in the upper layer, whereas $\mathcal{W}$ defines the power passed to the layer below.

It should be noted that the above classification is made with respect to the rate of change of the kinetic energy only. It is possible that the surface buoyancy forcing generates internal or gravitational potential energy and that this energy is converted into kinetic energy within the upper layer and leaves the layer via $\mathcal{W}$. In this case, $\mathcal{W}$ is not completely wind generated. A separation of the part of $\mathcal{W}$ resulting from the wind from the part resulting from the buoyancy forcing is beyond the scope of the present paper. In this study, $\mathcal{W}$ is assumed to be mainly a result of the wind and referred to as the wind-generated power available to the deep ocean.

The power considered by Wang and Huang (2004), Alford (2001), and Watanabe and Hibiya (2002) represents parts of $\mathcal{F}_s$, rather than $\mathcal{W}$. Wunsch (1998), on the other hand, considered an approximation of $\mathcal{W}$ using the following assumptions. First, it is assumed that $\mathcal{W}$ can be approximated by the power generated by the pressure via vertical velocity at the bottom of the layer at d,

$$\mathcal{W} \simeq \mathcal{P}_d. \tag{14}$$

The approximation is appropriate when $\mathcal{J}_d$ is negligible and when the level d is beneath the Ekman layer. The latter suggests that the shear-induced stress τ_d at d and from that $\mathcal{F}_d$ are negligible.

Second, Wunsch further approximates $\mathcal{P}_d$ by

$$\mathcal{P}_{\text{wunsch}} \equiv -\int_A (\overline{\tau_{s,x} u_{g,\eta}} + \overline{\tau_{s,y} v_{g,\eta}})\, dA, \tag{15}$$

where $(u_{g,\eta}, v_{g,\eta})$ is the geostrophic velocity derived from the sea surface height (SSH) η. Note that a different convention on the sign of z and w is used by Wunsch (1998). To approximate $\mathcal{P}_d$ by $\mathcal{P}_{\text{wunsch}}$, the sea surface is assumed to be rigid so that $\partial\eta/\partial t$ is zero and

$\mathcal{P}_{1,d}$ vanishes. Furthermore, the near-surface transport $\mathbf{U}$ in $\mathcal{P}_{2,d}$ has to be replaced by the net Ekman transport

$$\mathbf{U} = \mathbf{U}_e = \frac{1}{f\rho_o}\,\tau_s \times \mathbf{k}, \tag{16}$$

where $\mathbf{k}$ is the unit vector in the vertical direction. The condition that $\mathcal{P}_{2,d}$ in Eq. (9) is determined by $\mathbf{U} = \mathbf{U}_e$ implies that for $\mathbf{U}_g \equiv \mathbf{U} - \mathbf{U}_e$,

$$\int_A \overline{\mathbf{U}_g \cdot \nabla p_d}\, dA = 0. \tag{17}$$

Because

$$\mathbf{U}_g \cdot \nabla p_d = \int_z \mathbf{u}_g \cdot \nabla p_d\, dz = \int_z \left(\frac{1}{\rho_o f}\mathbf{k} \times \nabla p_z \cdot \nabla p_d\right) dz, \tag{18}$$

Eq. (17) is only satisfied when the geostrophic velocity $\mathbf{u}_g$ at z is determined by $\mathcal{P}_d$, rather than by p_z. The latter implies that the steric effect on the pressure is negligible, or equivalently that the geostrophic velocity is constant over the column of depth d and determined by

$$\nabla p_d = g\rho_o \nabla \eta. \tag{19}$$

Using Eqs. (16) and (19), $\mathcal{P}_{d,2}$ given in Eq. (9) reduces to $\mathcal{P}_{\text{wunsch}}$ given in Eq. (15), which is the approximation used by Wunsch (1998). Note that in contrast to $\mathcal{P}_{d,2}$, $\mathcal{P}_{\text{wunsch}}$ is not valid in the equatorial region where geostrophy breaks down.

Equating $\mathcal{W}$ to $\mathcal{P}_{\text{wunsch}}$ is equivalent to assuming that the upper layer is a vertically homogeneous Ekman layer that is described by the linear momentum equation without the advection term under the boundary conditions $w_s = 0$ at $z = 0$ and $\tau_d = 0$ at $z = d$. Section 4d assesses the range of the errors made when replacing $\mathcal{W}$ obtained from the primitive equations by $\mathcal{P}_{\text{wunsch}}$ obtained from the Ekman dynamics.

For the evaluation of $\mathcal{P}_d$, $\mathcal{P}_{d,1}$, and $\mathcal{P}_{d,2}$ pressure p is calculated as a function of depth from the hydrostatic relation using the in situ density obtained from the equation of state. The estimation of $\mathcal{F}_d$ requires the knowledge of the diffusivity coefficient K_m, which is not stored during the integration. To assess the magnitude of $\mathcal{F}_d$, an additional 1-month integration is carried out using the restart data from 1 January 2003. Only the January situation is indicated by $\mathcal{F}_d$ derived from these data.

The time-mean quantities $\mathcal{F}$, $\mathcal{J}_{d,1}$, $\mathcal{P}_{d,2}$, and $\mathcal{P}_d$ involve the time means of products of two variables, say xy. Express x in $x = \bar{x} + x'$, with $x' = x^* + x''$, where x' represents the deviation from the mean $\bar{x}$, x^* is the mean annual cycle, and x'' is the deviation of x' from x^*, and similarly for y. The time average of xy can be decomposed into

$$\overline{xy} = \overline{xy} + \overline{x'y'} = \overline{xy} + x^*y^* + \overline{x''y''}, \tag{20}$$

where $\overline{xy}$ is the contribution from the time means, and x^*y^* and $\overline{x''y''}$ are contributions from variations on seasonal and nonseasonal time scales, respectively. In the analysis given below, the quantities $\mathcal{F}$, $\mathcal{J}_{d,1}$, $\mathcal{P}_{d,2}$, and $\mathcal{P}_d$ are decomposed according to Eq. (20).

As described in the appendix, even though the 3-day snapshots can recover the total variances and covariances (i.e., $\overline{x^2}$ and $\overline{xy}$), they cannot completely recover the centered variances and covariances (i.e., $\overline{x'^2}$ and $\overline{x''y''}$) in the presence of the diurnal cycle. More precisely, the variances and covariances related to the diurnal cycle will be falsely recognized as the variances and covariances of the mean fields (i.e., $\overline{x^2}$ and $\overline{xy}$), rather than those of the time-varying components (i.e., $\overline{x'^2}$ and $\overline{x''y''}$). This shift of variance can be negligible if the variance of the diurnal cycle is much smaller than that related to the mean fields and to time-varying components on all time scales.

For the sake of computational efficiency, the analysis is applied to data on a $0.5° \times 0.5°$ grid obtained using a simple skipping method (i.e., taking every fifth grid point). To be sure that the skipping method does not induce substantial errors, the mean kinetic energy is calculated from the OFES data on the original $0.1° \times 0.1°$ grid and on the $0.5° \times 0.5°$ grid obtained using the skipping method. The error induced by coarsening is found to be smaller than 1% when integrated globally.

4. Results

a. Comparison with observations

Global and regional aspects of the circulation produced by the OFES model driven with the climatological fluxes were already compared with observations in Masumoto et al. (2004). Here the comparison concentrates on the pressure power given in Eq. (15) only. The same quantity was considered by Wunsch (1998) using the Ocean Topography Experiment (TOPEX)/Poseidon data and the wind stress from NCEP. His map of $\overline{\tau_{s,x}}\,\overline{u_{g,\eta}}$ (Fig. 2a in Wunsch 1998) shows a broad band of large positive values up to 24×10^{-3} W m^{-2} in the region of the Southern Ocean and negative values up to -6×10^{-3} W m^{-2} in the subtropical regions. His map of $\overline{\tau_{s,y}}\,\overline{v_{g,\eta}}$ (Fig. 2b in Wunsch 1998) shows patchy structures in the Southern Ocean and positive values in the eastern subtropics, in particular in the Atlantic.

The spatial structures of $\overline{\tau_{s,x}}\,\overline{u_{g,\eta}}$ and $\overline{\tau_{s,y}}\,\overline{v_{g,\eta}}$ obtained from the OFES data (Fig. 1) compare well to the result

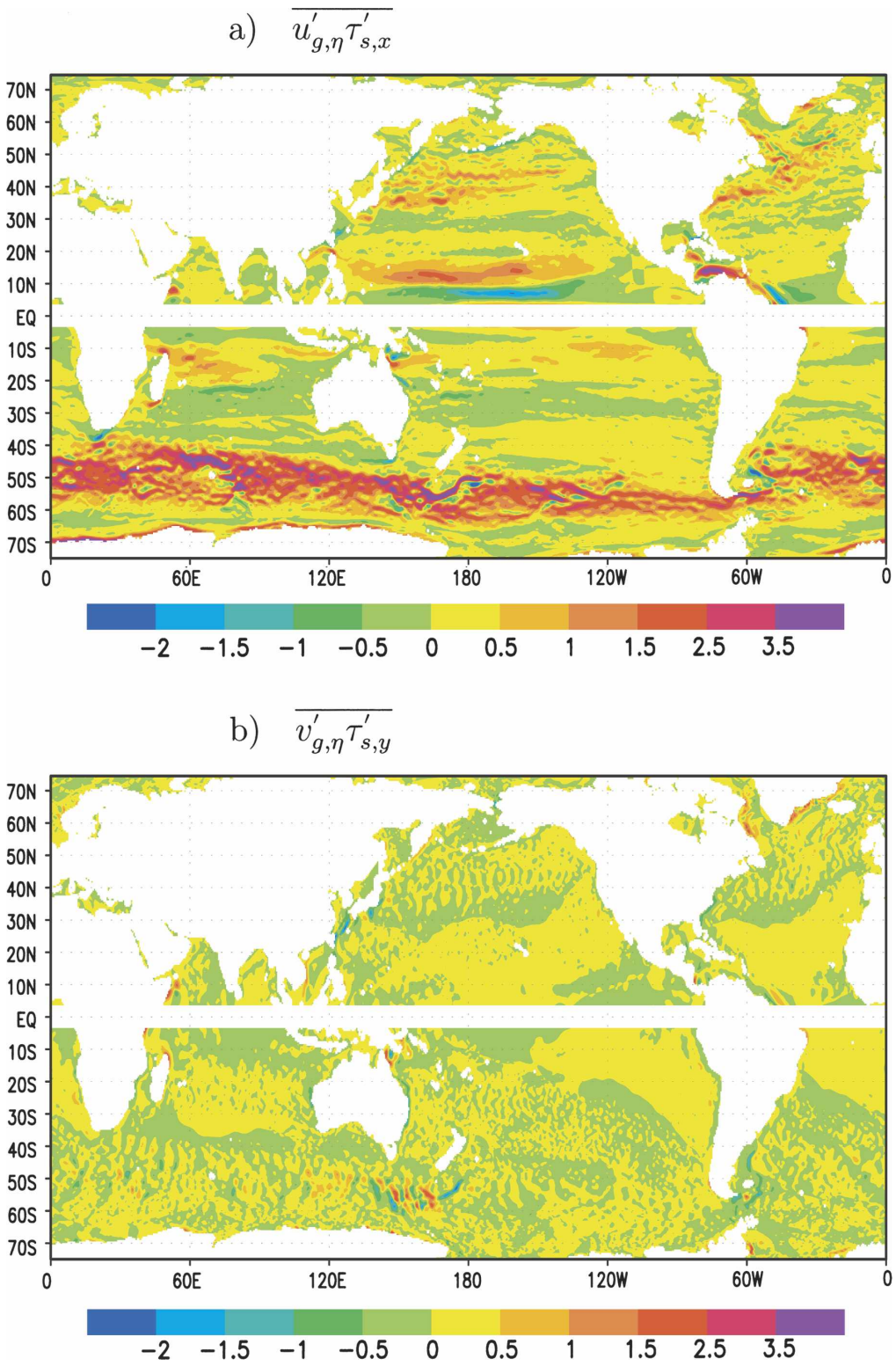

FIG. 1. Spatial distribution (10^{-3} W m^{-2}) of (a) $\overline{u_{g,\eta}}\,\overline{\tau_{s,x}}$ and (b) $\overline{v_{g,\eta}}\,\overline{\tau_{s,y}}$, where $u_{g,\eta}$ and $v_{g,\mathrm{ets}}$ are zonal and meridional geostrophic velocities derived from the sea surface height and $\tau_{s,x}$ and $\tau_{s,y}$ are zonal and meridional wind stress. The equatorial region within ±3° is excluded from the calculation.

of Wunsch (1998), not only with respect to the large positive values of $\overline{\tau_{s,x}}\ \overline{u_{g,\eta}}$ in the Southern Ocean, but also with respect to the dominance of the contribution from $\overline{\tau_{s,x}}\ \overline{u_{g,\eta}}$ relative to that from $\overline{\tau_{s,y}}\ \overline{v_{g,\eta}}$. The maximum in the Southern Ocean is, however, higher and reaches 40×10^{-3} W m^{-2} at a few locations. The largest difference is the strips of positive and negative values just north of the equator in the tropical Pacific, which are much less pronounced in Fig. 2a of Wunsch (1998). The globally integrated value of about 0.92 TW is somewhat higher than the 0.84 TW given by Wunsch.

The contributions from temporal variations $\overline{\tau'_{s,x}u'_{g,\eta}}$ and $\overline{\tau'_{s,y}v'_{g,\eta}}$ are shown in Fig. 2. In the Indian Ocean, the large values result mainly from the annual cycle. The distribution of these values compare also reasonably well to that by Wunsch (1998). In the mid- and high latitudes, Fig. 2 shows sequences of positive and negative values in the regions of Antarctic Circumpolar Current, Kuroshio, and Gulf Stream, which are not found in the respective figure by Wunsch (1998, his Fig. 3). Furthermore, $\overline{\tau'_{s,x}u'_{g,\eta}}$ derived by Wunsch shows a narrow band of negative values, which is absent in Fig. 2a. In general, the distributions in Wunsch (1998) are much smoother than those shown in Fig. 2. The global integral of about 0.14 TW is much smaller than that obtained from the time mean fields. It is notably larger than the value of 0.04 TW given by Wunsch.

Wunsch also represented an estimate using the model of Semtner and Chervin (1992) with the nominal ¼° horizontal resolution. The overall structure obtained from the OFES model is similar to that obtained from the model of Semtner and Chervin, including the sequences of positive and negative values related to $\overline{\tau'_{s,y}v'_{g,\eta}}$ in the regions of Antarctic Circumpolar Current, Kuroshio, and Gulf Stream. The main difference is the magnitudes. The OFES model produces larger maximum than the model by Semtner and Chervin.

b. Power provided by the wind at the sea surface: $\mathcal{F}_s$

Before estimating the power input to the deep ocean, consider first the question of how large the total wind-generated power is. Figure 3a shows $\overline{\mathbf{u}_s \cdot \tau_s}$, the total power generated by the wind at the sea surface. The power is stronger in the storm-track regions than in the subtropics. The largest magnitudes of up to 40×10^{-3} W m^{-2} are found over the Southern Ocean. Also shown in Fig. 3 are the contributions from the time-mean wind stress $\overline{\mathbf{u}}_s \cdot \overline{\tau}_s$ (Fig. 3b), and that from the nonseasonal time-varying stress $\overline{\mathbf{u}''_s \cdot \tau''_s}$ (Fig. 3c). The former has larger magnitudes than the latter. Nevertheless, the latter produces notable power when integrated globally. This is because $\overline{\mathbf{u}''_s \cdot \tau''_s}$ is positive everywhere, indicating that the power provided by the time-varying wind stress is directly used to generate the kinetic energy of time-varying currents. This cannot be said for the time-mean wind stress, given values of opposite signs in Fig. 3b. The contribution from seasonal variations results mainly from the Indian monsoon system with the largest values along the African coast (not shown).

Integrating over the sea surface of the model yields the net power supply of about 3.8 TW (second column in Table 2). About 2 TW of it (a little more than 50%) can be attributed to the time mean circulation, about 1.5 TW (about 40%) to the variations on the nonseasonal time scales, and about 0.3 TW (about 7%) to seasonal variations. Thus, nonseasonal time-varying wind stresses are not negligible in producing the net power at the sea surface.

Even though there is no direct estimate of $\mathcal{F}_s$ from observations, the total power provided by the wind is indicated by the sum of the power input to the surface geostrophic currents by Wunsch (1998), which is about 0.88 TW, and the power input to the surface ageostrophic currents by Wang and Huang (2004), which is about 2.3 TW. The sum of about 3.2 TW is in broad agreement with the value of 3.8 TW produced by the OFES model.

c. Power passed to the deep ocean: $\mathcal{W} = \mathcal{J}_d + \mathcal{P}_{d,1} + \mathcal{P}_{d,2} - \mathcal{F}_d$

Consider now the question of how much of the total power of 3.8 TW is passed to the ocean beneath the surface layer as given by $\mathcal{W}$. Here $\mathcal{W}$ consists of the energy flux across the bottom of the surface layer at d resulting from the nonlinear advection term $\mathcal{J}_d$, the power generated by the pressure at d, $\mathcal{P}_{d,1} + \mathcal{P}_{d,2}$, and the power generated by the stress at d, $-\mathcal{F}_d$. The energy flux $\mathcal{J}_d$ is about two orders of magnitude smaller than $\mathcal{F}_s$ for all values of d considered (not shown). Thus, the nonlinear advection term is extremely inefficient in passing the power generated at the surface to the deeper ocean. The pressure power associated with the tendency of the SSH term $\mathcal{P}_{d,1}$ is also negligible, at least when estimating $\mathcal{P}_d$ from 3-day snapshots. The validity of this result needs to be further clarified.

Substantial power is found for $\mathcal{P}_{d,2}$ generated by the pressure associated with the vertically integrated near-surface transport $\mathbf{U}$. However, $\mathcal{P}_{d,2}$ varies drastically with the depth d (black line in Fig. 4). At the bottom of the first model layer, that is, at $d = 5$ m, $\mathcal{P}_{d,2}$ is -0.08 TW and hence more than one order of magnitude smaller than $\mathcal{F}_s$. Here $\mathcal{P}_{d,2}$ is only substantial for d deeper than about 60 m and becomes more or less constant for d deeper than 80 m, with the largest value of about 0.99 TW. Thus, a little more than one-quarter of

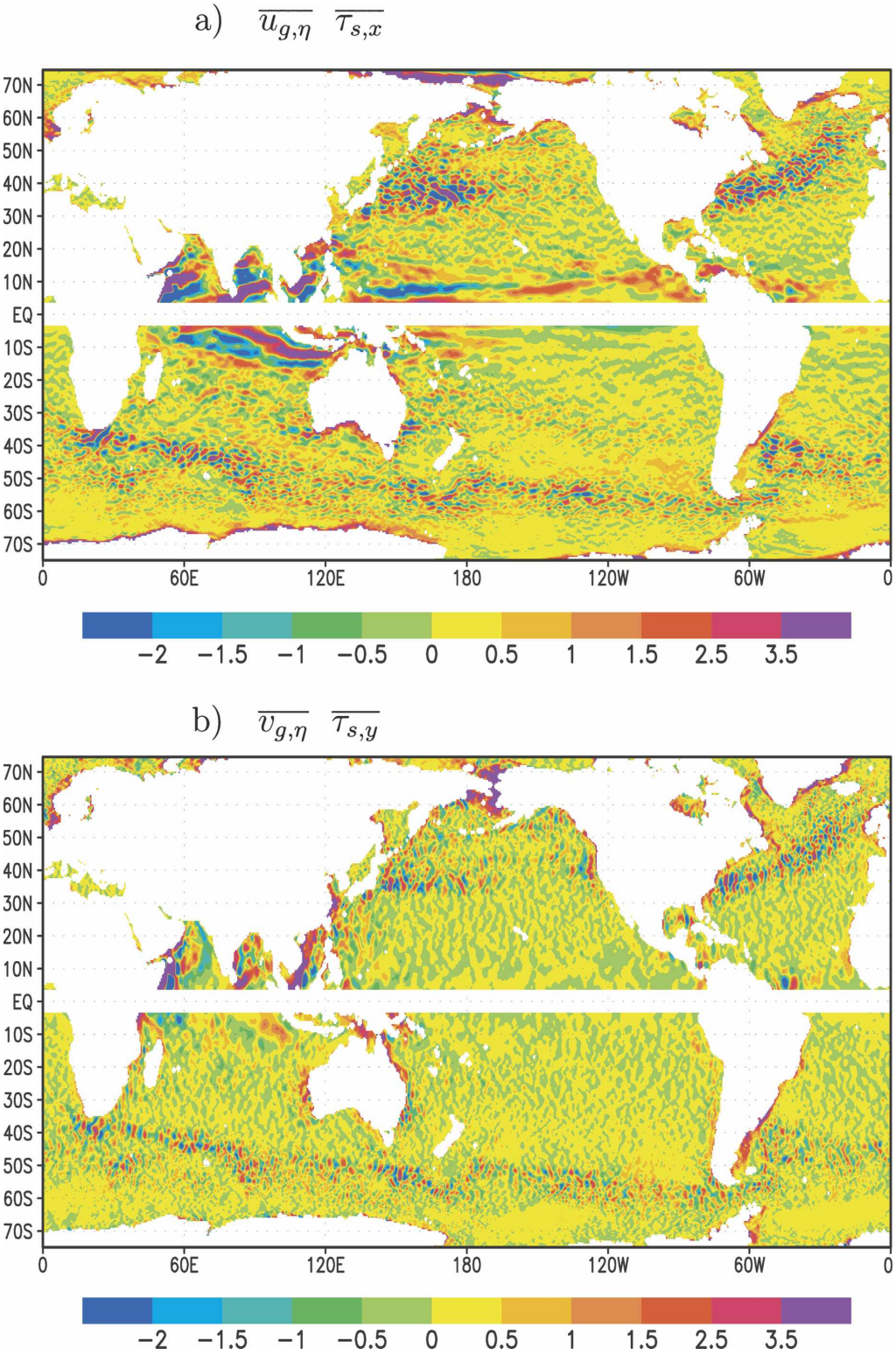

FIG. 2. As in Fig. 1, but for contributions from time-varying components (a) $\overline{u'_{g,\eta}\tau'_{s,x}}$ and (b) $\overline{v'_{g,\eta}\tau'_{s,y}}$.

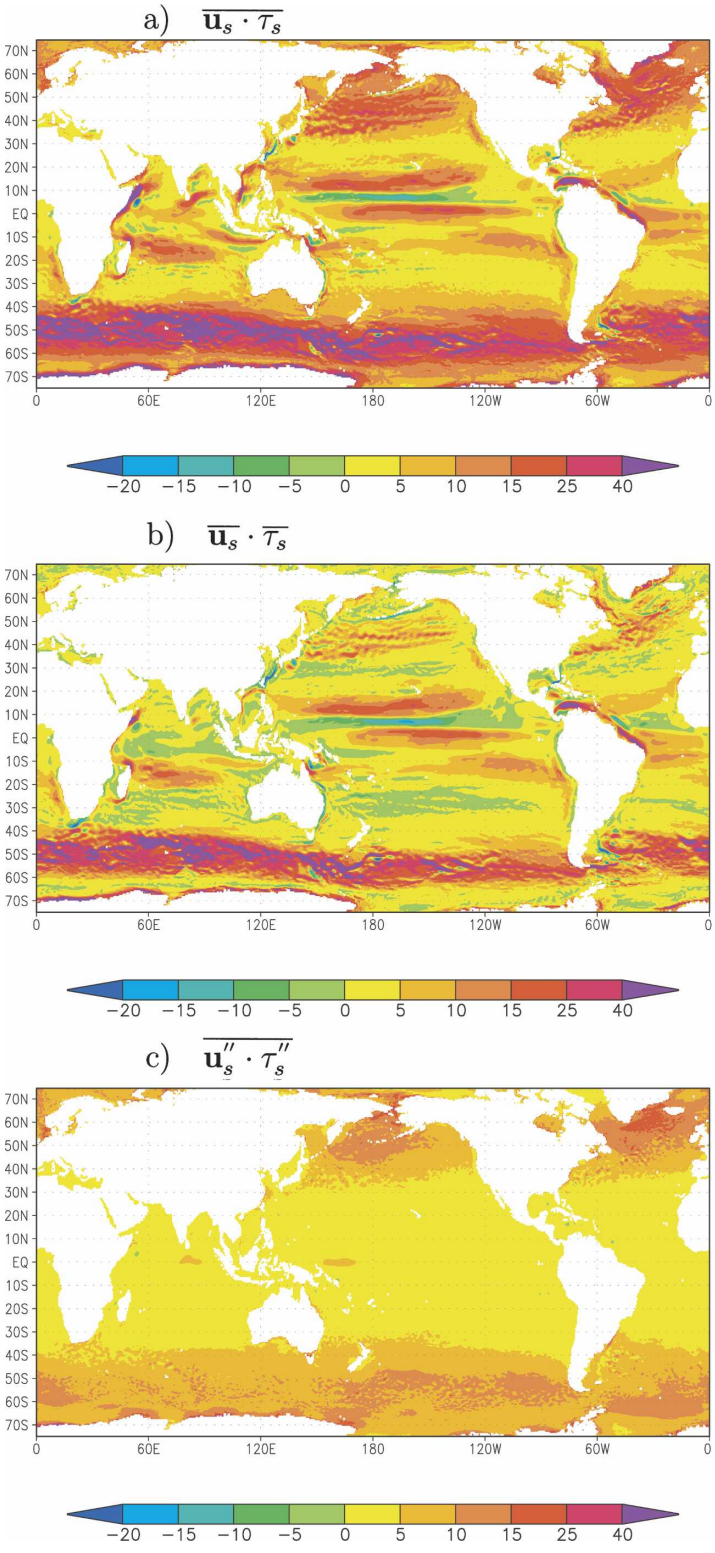

FIG. 3. Spatial distributions (10^{-3} W m^{-2}) of (a) $\overline{\mathbf{u}_s \cdot \tau_s}$, (b) $\overline{\mathbf{u}_s} \cdot \overline{\tau_s}$, and (c) $\overline{\mathbf{u}_s' \cdot \tau_s'}$, which contribute to the power generated by the wind $\mathcal{P}_s$.

TABLE 2. Magnitudes of the total power generated by the wind on the surface $\mathcal{F}_s$, and the amount of the total power that is passed through the surface layer of thickness $d = 110$ m, $\mathcal{W}$. Also shown is the approximation of $\mathcal{W}$ used by Wunsch (1998), $\mathcal{P}_{\text{wunsch}}$. The fluxes in the line labeled by $\overline{xy}$ are decomposed into contributions from the time means, $\overline{xy}$, from the annual cycle, x^*y^*, and from the variations on nonseasonal time scales, $\overline{x''y''}$. Note that the two digits after the decimal point do not imply an absolute accuracy of 0.01 TW. They are given to allow a comparison with the numbers of the same order given by Wunsch (1998).

		$\mathcal{W}$ (TW)				
	$\lvert\mathcal{F}_s\rvert$ (TW)	$\lvert\mathcal{J}_d\rvert$	$\lvert\mathcal{P}_{d,1}\rvert$	$\lvert\mathcal{P}_{d,2}\rvert$	$\lvert\mathcal{F}_d\rvert$	$\lvert\mathcal{P}_{\text{wunsch}}\rvert$
$\overline{xy}$	3.77	<0.01	<0.01	0.99	>0.14	1.06
$\overline{xy}$	1.98	<0.01	<0.01	0.94	—	0.92
x^*y^*	0.29	<0.01	<0.01	0.04	—	0.05
$\overline{x''y''}$	1.50	<0.01	<0.01	0.01	—	0.09

the wind power is passed through a layer of about 110-m thickness to the deep ocean by the pressure. When decomposing $\mathcal{P}_{d,2}$ into the contributions from the means (red line in Fig. 4) and variations (green lines in Fig. 4), one finds that the contribution from variations on seasonal and nonseasonal time scales is small and accounts only about 5% $\mathcal{P}_{d,2}$. The numbers for the surface layer of thickness $d = 110$ m are given in Table 2.

The vertical profile of $\mathcal{P}_{d,2}$ (black line in Fig. 4) shows surprisingly little dependence of $\mathcal{P}_{d,2}$ on d for d larger than, say, 80 m. This suggests that the conclusion that a little more than one-quarter of the wind power passes the surface layer and becomes available to the deep ocean is insensitive to the precise depth of the surface layer.

Consider now the spatial distribution of $\mathcal{P}_{d,2}$ for $d = 114$ m shown in Fig. 5. Negative values indicate the power passed to the ocean below the surface layer. Large negative values are found in the subtropical oceans and in the region of the Antarctic Circumpolar Current. There are spots of positive values in the region of the Antarctic Circumpolar Current. More large positive values are found in the region of the Gulf Stream and the Kuroshio.

To quantify the last term in $\mathcal{W}$, $\mathcal{F}_d$, one needs to know the coefficient K_m. The extra integration for January 2003 suggests that K_m is highly inhomogeneous in space, in particular in the deeper layers. For instance, K_m below the first model layer is mostly larger than 50 $\text{cm}^2\,\text{s}^{-1}$ with extreme values of about 300–400 $\text{cm}^2\,\text{s}^{-1}$ in the storm-track regions. In the 13th or 14th model layer, however, K_m is mostly smaller than 50 $\text{cm}^2\,\text{s}^{-1}$, but with extreme values of about 10^3–10^4 $\text{cm}^2\,\text{s}^{-1}$ in the North Atlantic and North Pacific. It is this spatial structure of K_m that determines the pattern of the shear-induced power shown in Fig. 6. The strips of values up

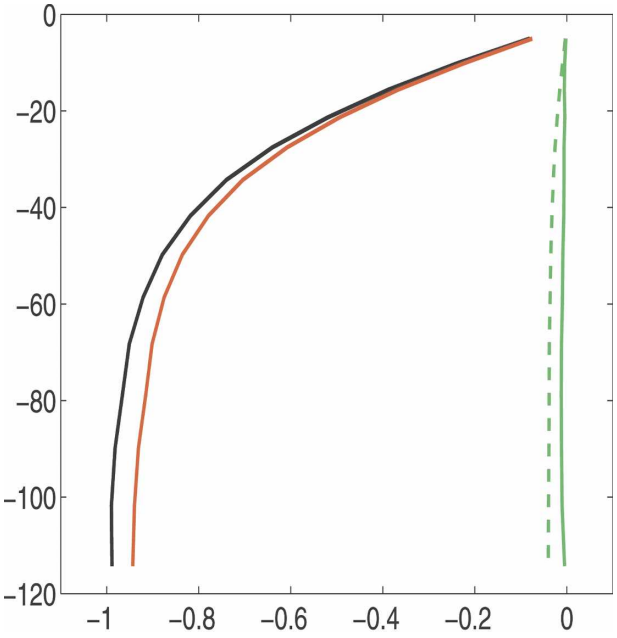

FIG. 4. The pressure power $\mathcal{P}_{d,2}$ in 10^{12} W as a function of depth d (black line), and contributions to $\mathcal{P}_{d,2}$ from the time means (red) and variations on seasonal (green dashed) and nonseasonal (green solid) time scales.

to 20×10^{-3} W m^{-2} in the North Pacific and in the North Atlantic result from these extremes of K_m. The extremes are consistent with the fact that the boundary layer is deeper than 300 m there (Fig. 7a). The boundary layer depth is provided by the KPP implemented in the OFES model. One may conclude that the shear-induced stress is able to produce substantial power, if the depth of the surface layer d lies inside the boundary layer.

Integrating values in Fig. 6 over the entire ocean area yields an $\mathcal{F}_d$ of about −0.14 TW for January 2003 (Table 2). The magnitude of $\mathcal{F}_d$ can be somewhat larger than 0.14 TW when considering the annual condition. This is because the boundary layer depth in July 2003 is deeper than 110 m over large areas in the Southern Ocean (Fig. 7b), so that K_m, and from that the power exerted by shear-induced stress, can be substantial there.

Figure 8 shows $-\mathcal{F}_d$ as a function of d, as derived from the extra integration for January 2003. The shear-induced stress produces power of about 3.57 TW at the bottom of the first model layer at 5 m, which is about 95% of the wind power at the sea surface. With increasing d, the power generated by the shear-induced stress drastically decreases. At the depth of about 50 m $\mathcal{F}_d$ reduces to less than 0.5 TW.

One may conclude that among the four terms that contribute to $\mathcal{W}$, only the contributions from the pressure and the shear-induced stress are significant. The

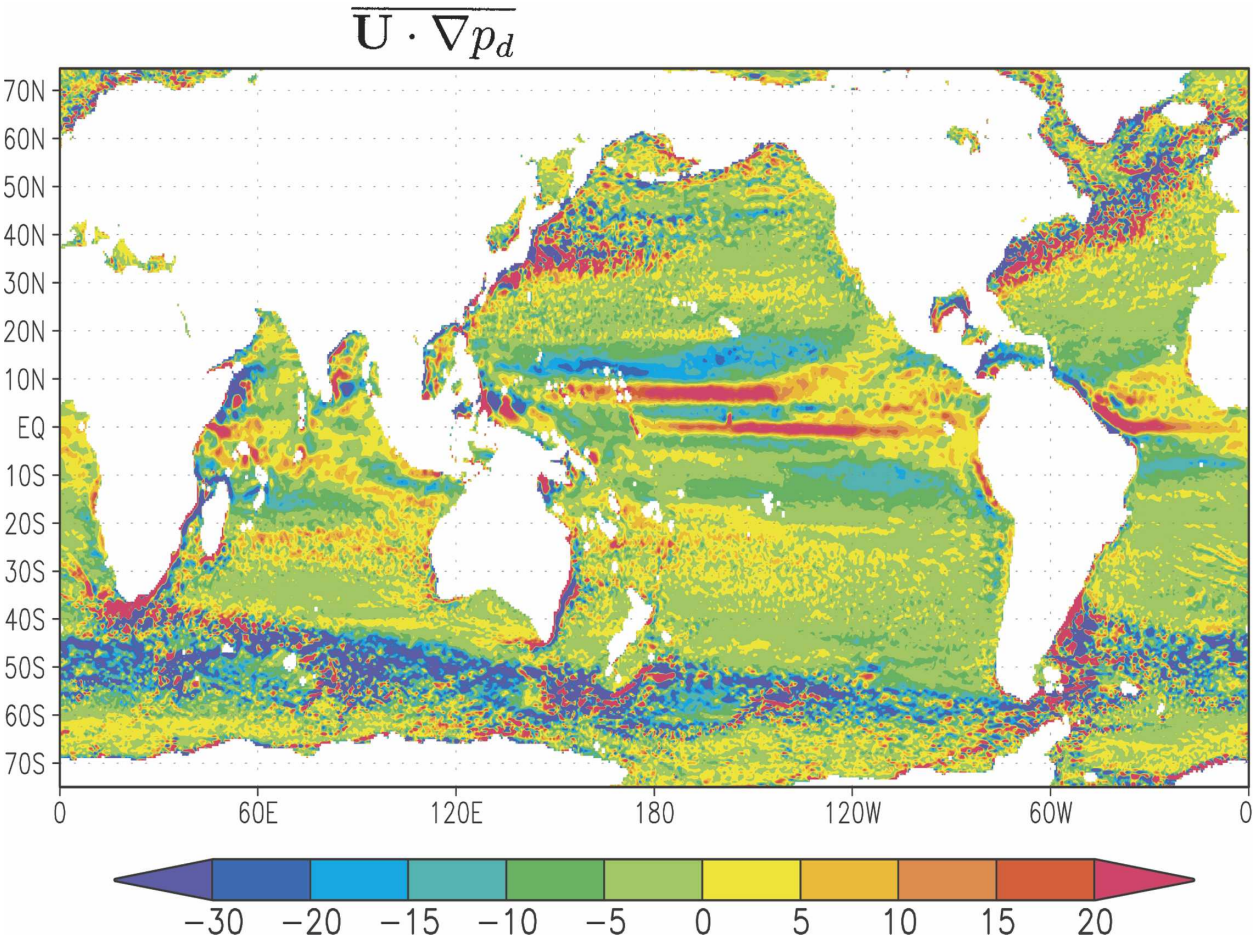

FIG. 5. Spatial distribution (10^{-3} W m^{-2}) of $\overline{\mathbf{U} \cdot \nabla p_d}$, which gives rise to the pressure power $\mathcal{P}_{d,2}$ at depth $d = 114$ m.

pressure term dominates in the Southern Ocean below about 80 m. The shear-induced stress dominates in the layer just below the surface and is only notable below a surface layer of about 50 m where K_m is extremely large.

d. *Validity of assumptions used to approximate* $\mathcal{W}$ by $\mathcal{P}_{wunsch}$

The OFES data suggest that $\mathcal{J}_d$ and $\mathcal{P}_{d,1}$ are negligible. Consequently, if $\mathcal{J}_d$ is also negligible, one would have $\mathcal{W} \simeq \mathcal{P}_{d,2}$. The $\mathcal{P}_{d,2}$ can be further approximated by $\mathcal{P}_{\text{wunsch}}$ when assuming that the near-surface transport $\mathbf{U}$ equals the Ekman transport given in Eq. (16) and that the steric effect is negligible so that the pressure gradient can be replaced by the gradient of the SSH given in Eq. (19). The assumptions induce errors, whose magnitudes depend on the choice of d. If d is chosen to be the averaged boundary layer depth, one would have substantial contributions from the shear-induced stress in regions where the boundary layer is deeper than d. It would not be appropriate to replace the near-surface transport $\mathbf{U}$ by the Ekman transport $\mathbf{U}_e$ using Eq. (16). To avoid this, one may choose d to be completely below the boundary layer. This can, however, make assumption Eq. (19) be inappropriate, because an increase in d leads to an increase in the steric effect on pressure.

To assess the magnitude of errors induced by using Eqs. (16) and (19), the power generated by the pressure is calculated by replacing in Eq. (9) $\mathbf{U}$ by the Ekman transport using Eq. (16) and ∇p_d by the expression in Eq. (19). The resulting pressure power is shown by the dashed and dot–dashed lines in Fig. 9, respectively. The solid line shows $\mathcal{P}_{d,2}$.

The error related to Eq. (16) is indicated by the difference between the dashed and solid curves. The difference is extremely large in the first 30–40 m, because the Ekman transport occurs in a layer much thicker than 30–40 m. With increasing depth, the difference decreases. For d deeper than about 80 m, the decrease in the difference is more or less halted and reaches a nonzero value. This suggests that even when consider-

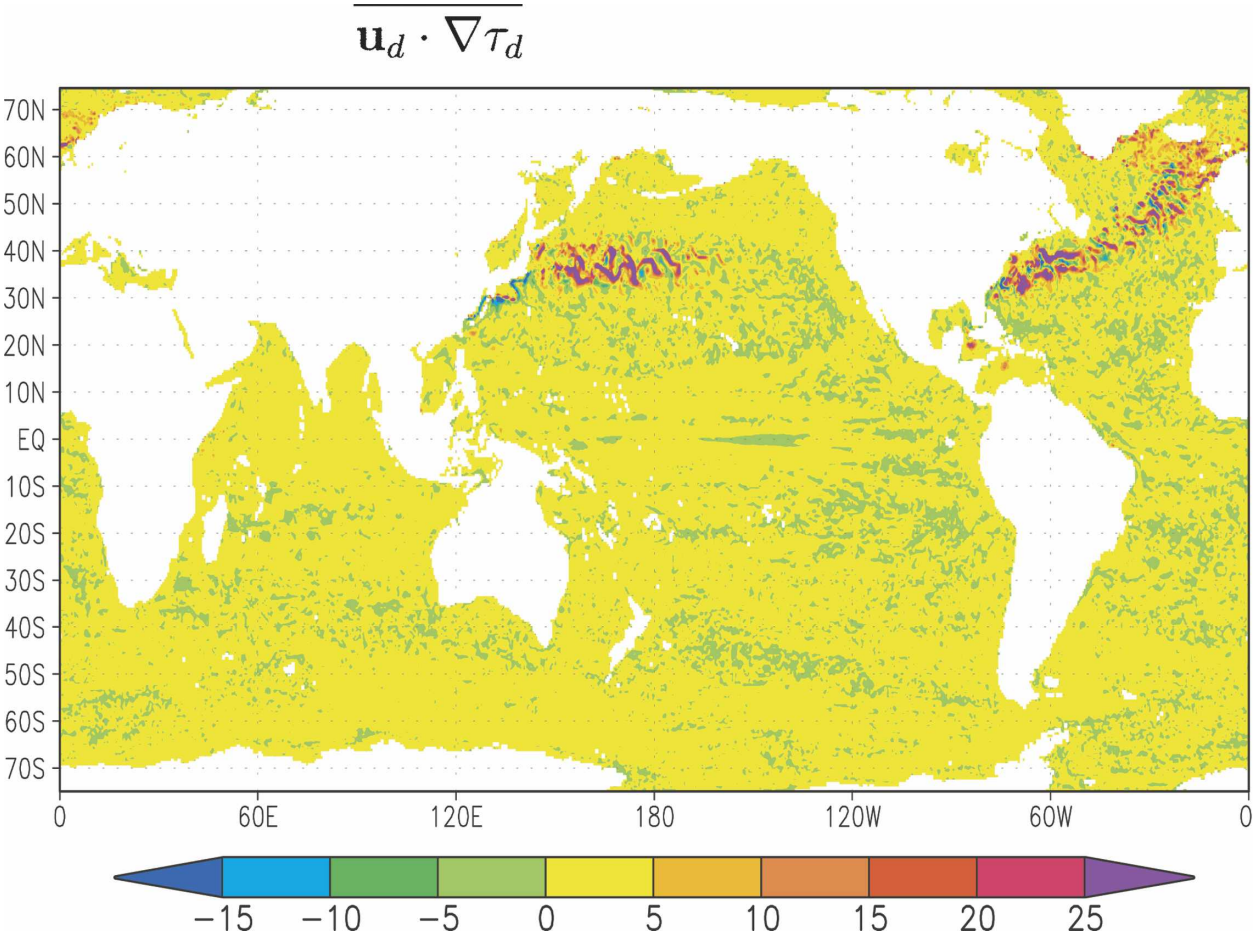

FIG. 6. Spatial distribution (10^{-3} W m^{-2}) of $\overline{\mathbf{u}_d \cdot \nabla \tau_d}$, which gives rise to the power generated by the shear-induced stress at depth $d = 101$ m for January 2003.

ing a layer notably thicker than 110 m, the transport $\mathbf{U}$ will still be smaller than the Ekman transport $\mathbf{U}_e$. This will happen if the shear-induced stress τ_d does not completely diminish in the oceanic interior. With τ_d being nonzero at z anywhere in the oceanic interior, the transport $\mathbf{U}$ integrated from the surface to z will not be identical to the total Ekman transport, even when the momentum equation is well described by the Ekman dynamics from the surface down to z. At $z = 110$ m, replacing the near-surface transport with the Ekman transport using Eq. (16) leads to an overestimate of $\mathcal{P}_{d,2}$ of about 0.2 TW.

The error induced by neglecting the steric effect according to Eq. (19) is indicated by the difference between the dot–dashed and solid lines. As the steric effect becomes more notable for a large value of d, the errors induced by assumption Eq. (19) increase with increasing d, leading to an underestimate by about 0.1 TW at $d = 110$ m.

In general, one faces the problem that if one chooses d as deep as possible to avoid errors originating from the nonzero turbulent stress τ_d, one would have notable errors associated with the steric effect. If, on the other hand, one chooses d to be shallow to avoid the errors associated with the steric effect, one would have notable errors associated with τ_d. Fortunately, the two types of errors are of opposite signs and cancel each other to a large extent, at least at about 110-m depth. Figure 9 suggests that the net error is smaller than 10% when approximating $\mathcal{W}$ using $\mathcal{P}_{\text{wunsch}}$.

5. Discussion and conclusions

The analysis based on the OFES output addresses two issues that cannot, at least at the moment, be studied using observational data alone. First, it indicates how the wind-generated power is passed through a surface layer to the ocean beneath. The passage is accomplished essentially via the shear-induced stress ($\mathcal{F}_d$) and via pressure ($\mathcal{P}_d$). The energy flux that originates from nonlinear advection ($\mathcal{F}_d$) is unable to transport a no-

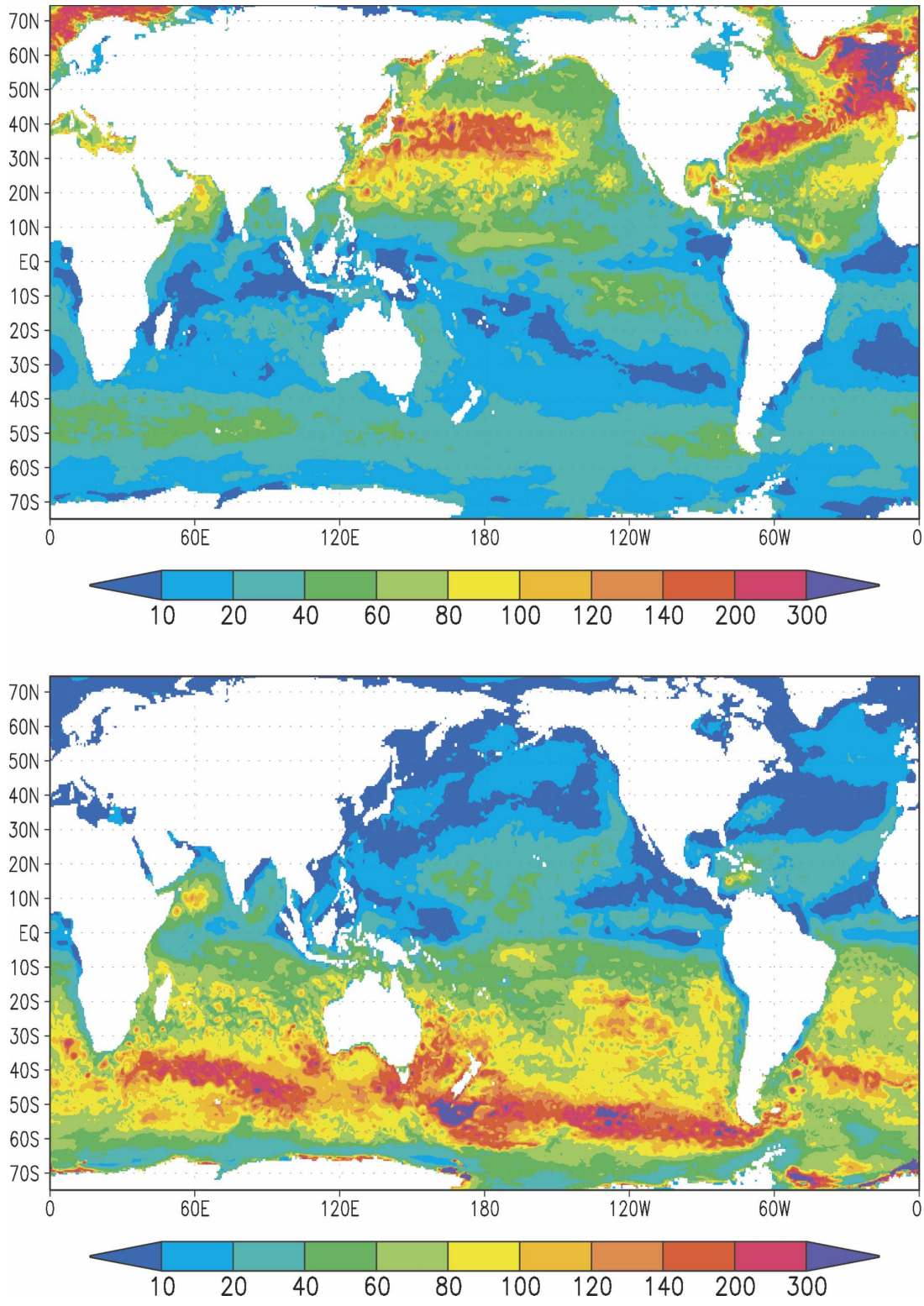

FIG. 7. Spatial distribution of the monthly mean boundary layer depth in meters for (a) January and (b) July 2003.

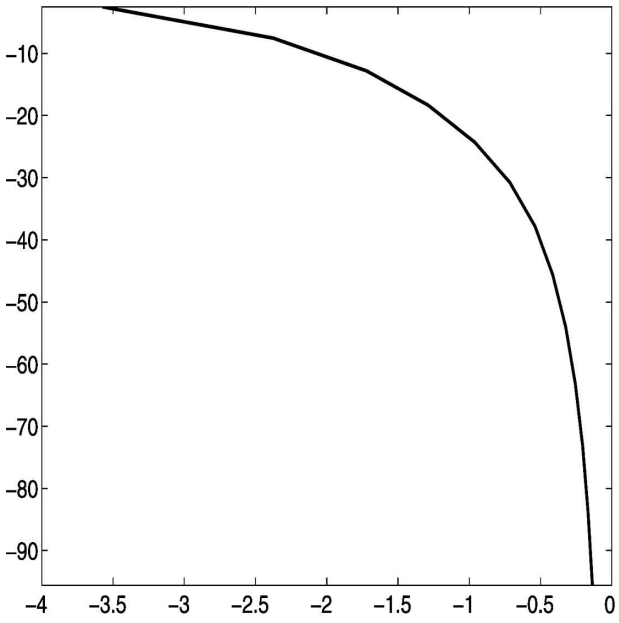

FIG. 8. The area-integrated power $-\mathcal{F}_d$ (10^{12} W), generated by the shear-induced stress as a function of depth d for January 2003.

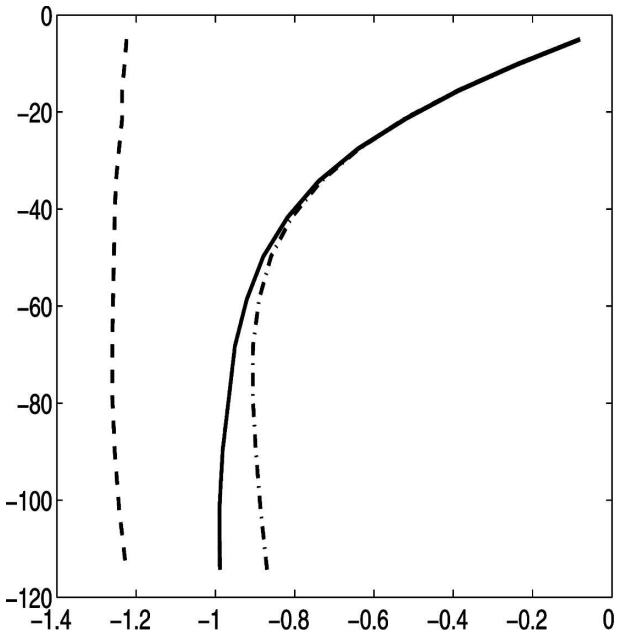

FIG. 9. The pressure power $\mathcal{P}_{d,2}$ (solid line) and two approximations of $\mathcal{P}_{d,2}$ obtained by replacing the near-surface transport **U** by the Ekman transport using Eq. (16) (dashed line) and by replacing the pressure gradient by the gradient of the sea surface height using Eq. (19) (dot–dashed line).

table amount of power downward. The roles of $\mathcal{F}_d$ and $\mathcal{P}_d$, in passing the wind power downward, exchange within the surface layer. Directly below the surface, the wind-generated power is passed down by the shear-induced stress only. As the distance to the surface increases, the dominance of the shear-induced stress weakens and the wind power is essentially passed down through the pressure via vertical velocity. The latter reaches a global value of about 1 TW for a surface layer of about 110-m thickness. At this level, the power generated by the shear-induced stress is reduced to about 0.1–0.2 TW.

Second, the present work assesses the range of errors made when simplifying the power available to the deep-ocean $\mathcal{W}$ using various assumptions. The errors arising from the assumption of zero vertical velocity at the sea surface and vanishing nonlinear advection term in the momentum equation are about one to two magnitudes smaller than $\mathcal{W}$, and are hence irrelevant. Notable errors are found when replacing the near-surface transport by the Ekman transport and when neglecting the steric effect. These two errors reach about 20% of $\mathcal{W}$. Nonetheless, the net error is small because the two errors have opposite signs and cancel each other to a large extent.

Based on the analysis of the OFES output, we conclude the following:

- The total power $\mathcal{W}$ generated by the wind at the sea surface is about 3.8 TW; one-half of the total power results from the time-mean wind stress and the other one-half from the time-varying wind stress.
- About 70% of the total power is dissipated or converted into potential energy within the surface layer of about 110-m thickness; the other 30%, about 1.1 TW, is passed to the ocean beneath. The number 1.1 TW is insensitive to the precise depth of the surface layer.
- The pressure power, which makes the largest contribution to $\mathcal{W}$, results essentially from the time-mean pressure and time-mean vertical velocity. The contribution from the transients is small.
- The net error arising from approximating $\mathcal{W}$ using the Ekman dynamics is less than 0.1 TW.

Acknowledgments. We thank the Earth Simulator Center for providing the OFES data, the two reviewers for constructive comments that greatly improved the paper, and Francis Zwiers for reviewing the appendix.

APPENDIX

Variances and Covariances of Sampled Processes

a. Total variances and covariances

Consider processes $x(t)$ and $y(t)$ and sampled processes $X_t = x(t\Delta t)$ and $Y_t = y(t\Delta t)$, which are obtained

by sampling $x(t)$ and $y(t)$, respectively, using the sampling interval Δt. The following shows that the variance of $X(t)$ equals the variance of $x(t)$, and the covariance between the sampled processes X_t and Y_t equals the covariance between $x(t)$ and $y(t)$. Because of these equalities, the mean kinetic energy balance, which describes a balance between quantities representing the total variances and covariances, can in principle be well estimated from snapshots obtained by sampling model output every a few days.

The proof follows the consideration of Priestley (1981), which assumes that $x(t)$ has the spectral representation

$$x(t) = \int_{-\infty}^{\infty} e^{it\omega}\, dZ_x(\omega). \tag{A1}$$

Using the identity

$$\int_{-\infty}^{\infty} \cdot\, d\omega = \sum_{k=-\infty}^{\infty} \int_{(2k-1)\pi/\Delta t}^{(2k+1)\pi/\Delta t} \cdot\, d\omega = \sum_{k=-\infty}^{\infty} \int_{-\pi/\Delta t}^{\pi/\Delta t} \cdot\, d\left(\omega + \frac{2k\pi}{\Delta t}\right), \tag{A2}$$

Priestley showed that the sampled process X_t is described by

$$X_t = \int_{-\pi/\Delta t}^{\pi/\Delta t} e^{it\Delta t\omega}\, dZ_X(\omega), \tag{A3}$$

with

$$dZ_X(\omega) = \sum_{k=-\infty}^{\infty} dZ_x\left(\omega + \frac{2k\pi}{\Delta t}\right), \quad \omega \le \pi/\Delta t. \tag{A4}$$

Equation (A4) describes the aliasing induced by sampling. It forms the basis of the folding principle illustrated in Fig. 7.1 in Priestley (1981). Similar spectral representations hold for $y(t)$ and the respective sampled process Y_t.

The total variance (covariance) is obtained by integrating the spectrum (cross spectrum) over the whole frequency domain. The frequency domain resolved by $x(t)$ is $[-\infty, \infty]$ and that by the sampled process X_t is $[-\pi/\Delta t, \pi/\Delta t]$. Hence, one has for the variances

$$\mathrm{var}(x) = \int_{-\infty}^{\infty} dH_x(\omega) \quad \text{and} \quad \mathrm{var}(X) = \int_{-\pi/\Delta t}^{\pi/\Delta t} dH_X(\omega), \tag{A5}$$

and for the covariances

$$\mathrm{cov}(xy) = \int_{-\infty}^{\infty} dH_{xy}(\omega) \quad \text{and} \quad \mathrm{cov}(XY) = \int_{-\pi/\Delta t}^{\pi/\Delta t} dH_{XY}(\omega), \tag{A6}$$

where the integrated spectra H_x and H_X are defined by

$$dH_x(\omega) = E[|dZ_x(\omega)|^2] \quad \text{and} \quad dH_X(\omega) = E[|dZ_X(\omega)|^2], \tag{A7}$$

and the integrated cross-spectra H_{xy} and H_{XY} are defined by

$$dH_{xy}(\omega) = E[dZ_x^*(\omega) dZ_y(\omega)] \quad \text{and} \quad dH_{XY}(\omega) = E[dZ_X^*(\omega) dZ_Y(\omega)]. \tag{A8}$$

Here E is the expectation and the asterisk indicates the complex conjugate.

To prove that the two variances in Eq. (A5) are equal, one takes the expectation of the square of Eq. (A4). Substituting the result into the definition of $\mathrm{var}(X)$ in Eq. (A5) yields

$$\mathrm{var}(X) = \int_{-\pi/\Delta t}^{\pi/\Delta t} dH_X(\omega) = \int_{-\pi/\Delta t}^{\pi/\Delta t} \sum_{k=-\infty}^{\infty} dH_x\left(\omega + \frac{2k\pi}{\Delta t}\right) = \int_{-\infty}^{\infty} dH_x(\omega) = \mathrm{var}(x), \tag{A9}$$

where Eq. (A2) and the orthogonality properties of $dZ_x(\omega)$ are used.

To prove that the two covariances in Eq. (A6) are equal, one takes the expectation of the product of the spectral representations of X and Y. Substituting the result into the definition of $\mathrm{cov}(XY)$, one finds

$$\mathrm{cov}(XY) = \int_{-\pi/\Delta t}^{\pi/\Delta t} dH_{XY}(\omega) = \int_{-\pi/\Delta t}^{\pi/\Delta t} \sum_{k=-\infty}^{\infty} dH_{xy}\left(\omega + \frac{2k\pi}{\Delta t}\right) = \int_{-\infty}^{\infty} dH_{xy}(\omega) = \mathrm{cov}(xy), \tag{A10}$$

where Eq. (A2) and the cross-orthogonality properties of $dZ_x(\omega)$ and $dZ_y(\omega)$ are used.

Equations (A9) and (A10) are a direct consequence of the folding principle (Fig. 7.1 of Priestley 1981). Because every spectral component $dH_x(\omega)$ at frequencies higher than the Nyquist frequency will be folded once into the frequency range lower than the Nyquist frequency with unchanged amplitudes, the total variance of $x(t)$ will be completely recovered by X_t. Similarly, the

total covariance between x and y will be completely recovered by X_t and Y_t.

b. Centered variances and covariances

The recovering of the total variances and covariances does not automatically imply a recovering of the centered variances and covariances (i.e., variances and covariances of anomalies obtained after removing the mean). In the present paper, the centered variances and covariances come into play when one decomposes the total mean kinetic energy balance into balances related to the mean fields and transient fields.

The following focuses on the variances. Similar consideration can be carried out for covariances. Denoting the centered variance by σ^2 and the mean by μ, one has

$$\sigma_x^2 + \mu_x^2 = \mathrm{var}(x) = \mathrm{var}(X) = \sigma_X^2 + \mu_X^2. \quad \text{(A11)}$$

If x represents velocity, $\mathrm{var}(x)$ gives the total mean kinetic energy, σ_x^2 is the energy related to the transients, and μ_x^2 is the energy related to the mean velocity field.

The centered variances will be recovered if sampling does not change the mean. When $x(t)$ contains deterministic oscillations, the mean is not changed as long as the aliased frequency is not zero. When $x(t)$ contains random oscillations such that $E[dZ_x(\omega)] = 0$ for all $\omega \neq 0$, the mean is not changed, even when oscillations in $x(t)$ are aliased into zero frequency, because the expectation of the aliased spectral components vanishes. Because of randomness in the wind forcing and dissipation processes, the inertial oscillations generated by the OFES model could be such random oscillations.

The centered variances will not be completely recovered if sampling changes the mean. This happens when a deterministic oscillation is aliased into frequency zero. As an example, consider $x(t)$, which contains a deterministic diurnal oscillation with period 24 h and zero time mean. Here X_t is obtained by sampling $x(t)$ every 24 h, or every 3×24 h as the OFES output. In this case, the sampled process misplaces the variance of the diurnal oscillation to the portion of the total variance related to the mean, rather than to that related to the transients.

c. Summary

From a theoretical point of view, the total mean kinetic energy balance can be completely recovered from sampled processes. Care must be taken when decomposing the total balance into contributions from the mean and transients. When using 3-day snapshots in the presence of the diurnal cycle, the contribution from the mean is overestimated and that from the transients is underestimated by the amount of the variance of the diurnal cycle. In practice, this difference may not be noticeable because of the smallness of the variance of the diurnal cycle relative to the variance related to the mean circulation and that related to the transients over a vast range of frequencies.

REFERENCES

Alford, M. H., 2001: Internal swell generation: The spatial distribution of energy flux from the wind to mixed layer near-inertial motions. *J. Phys. Oceanogr.,* **31,** 2359–2368.

Budyko, M. S., 1974: *Climate and Life*. Academic Press, 508 pp.

Large, W. G., J. C. McWilliams, and S. C. Doney, 1994: Oceanic vertical mixing: A review and a model with a nonlocal boundary layer parameterization. *Rev. Geophys.,* **32,** 363–403.

Masumoto, Y., and Coauthors, 2004: A fifty-year eddy-resolving simulation of the World Ocean—Preliminary outcomes of OFES (OGCM for the Earth Simulator). *J. Earth Simul.,* **1,** 35–56.

Munk, W., and C. Wunsch, 1998: Abyssal recipes II: Energetics of tidal and wind mixing. *Deep-Sea Res.,* **45,** 1976–2009.

Pacanowski, R. C., and S. M. Griffies, 2000: MOM 3.0 manual. NOAA/Geophysical Fluid Dynamics Laboratory, 680 pp.

Priestley, M. B., 1981: *Spectral Analysis and Time Series*. Academic Press, 890 pp.

Rosati, A., and K. Miyakoda, 1988: A general circulation model for upper ocean circulation. *J. Phys. Oceanogr.,* **18,** 1601–1626.

Semtner, A. J., Jr., and R. M. Chervin, 1992: Ocean general circulation from a global eddy-resolving model. *J. Geophys. Res.,* **97,** 5493–5550.

Stern, M. E., 1975: *Ocean Circulation Physics*. Academic Press, 275 pp.

Wang, W., and R. X. Huang, 2004: Wind energy input to the Ekman layer. *J. Phys. Oceanogr.,* **34,** 1267–1275.

Watanabe, M., and T. Hibiya, 2002: Global estimates of the wind-induced energy flux to inertial motions in the surface mixed layer. *Geophys. Res. Lett.,* **29,** 1239, doi:10.1029/2001GL014422.

Wunsch, C., 1998: The work done by the wind on the oceanic general circulation. *J. Phys. Oceanogr.,* **28,** 2332–2340.